ACS APPLIED MATERIALS & INTERFACES

Research Article

www.acsami.org

Simple Approach to Superhydrophobic Nanostructured Al for Practical Antifrosting Application Based on Enhanced Self-propelled Jumping Droplets

Aeree Kim,[†] Chan Lee,[†] Hyungmo Kim,[‡] and Joonwon Kim*,[†]

[†]Department of Mechanical Engineering, POSTECH, Pohang, 790-784, Republic of Korea

[‡]Korea Atomic Energy Research Institute (KAERI), Daejeon, 305-353, Republic of Korea

Supporting Information

ABSTRACT: Frost formation can cause operational difficulty and efficiency loss for many facilities such as aircraft, wind turbines, and outdoor heat exchangers. Self-propelled jumping by condensate droplets on superhydrophobic surfaces delays frost formation, so many attempts have been made to exploit this phenomenon. However, practical application of this phenomenon is currently unfeasible because many processes to fabricate the superhydrophobic surfaces are inefficient and because self-propelled jumping is difficult to be achieved in a humid and low-temperature environment because superhydrophobicity is degraded in these conditions. Here, we achieved significantly effective anti-icing superhydrophobic aluminum. Its extremely low adhesive properties allow self-propelled jumping under highly supersaturated conditions of high humidity or low surface temperature. As a result, this surface helps retard frost formation at that condition. The aluminum was made superhydrophobic by a simple and cost-effective process that is adaptable to any shape. Therefore, it has promise for use in practical and industrial applications.

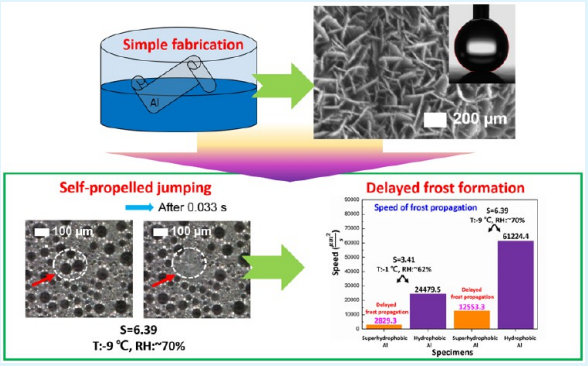

KEYWORDS: *superhydrophobic, self-propelled jumping, aluminum, anti-icing, antifrosting*

1. INTRODUCTION

Frost formation can cause serious economic and safety problems on facilities such as power lines, dams, aircraft, and heat exchangers.[1−4] Especially, frost formation on a heat exchanger causes serious efficiency decline.[5] For example, air-source heat pumps are usually placed outdoors to heat interior spaces and water; these pumps lose significant efficiency in cold climates because frost layers have an insulating effect and can increase the pressure drop in channels.[5−7] Once the condensate droplets freeze to form a frost layer, impinging water droplets like rain drops freeze immediately when they touch it, and this process may exacerbate icing problems. In addition, removing this frost layer is costly and requires much energy.[6] Therefore, practical approaches to prevent frosting should be developed.

Current active ice-mitigation methods include chemical treatment using chemicals (e.g., glycol) or physical treatment breaking already-formed ice layers.[3,8] These approaches require substantial energy, cause corrosion, and can harm the environment.[4,8,9] Recently, many researchers have been trying to develop anti-icing methods by preparing modified surfaces that delay or prevent freezing of condensed or impinging droplets.[10−12] Use of a superhydrophobic surface is a candidate method to solve the icing problem because an extremely low adhesive superhydrophobic surface enables impacting droplets to bounce off the surface before ice nucleation can occur and because trapped air inside structures of a superhydrophobic surface form insulation, which retards freezing.[13−16]

Coalescence-induced self-propelled jumping (SPJ) by condensate droplets that occurs on the superhydrophobic surface is also considered to be a key feature to prevent icing.[17−19] SPJ is the phenomenon in which coalescence droplets "jump" off the surface when they merge. SPJ occurs due to the release of excess surface energy on the weakly adhesive superhydrophobic surface.[20−22] SPJ by condensate droplets can retard frost formation.[3] However, SPJ shows significant dependency on the supersaturation $S = P_V/P_W$, where P_V is the vapor pressure and P_W is the saturation pressure that corresponds to the specimen surface temperature.[20] S is a useful factor to estimate the rate of the condensation. As S increases (due to increasing humidity or decreasing substrate temperature), the formation of condensate droplets increases on all structures of a superhydrophobic surface. Therefore, because of increased wettability, SPJ would not be observed at high S, although this motion is achieved at low S.[20] In reality, many situations experience high humidity and low temperature, so S is high in many situations. Therefore, achieving anti-icing

Received: January 11, 2015
Accepted: March 17, 2015
Published: March 17, 2015

DOI: 10.1021/acsami.5b00292
ACS Appl. Mater. Interfaces 2015, 7, 7206−7213

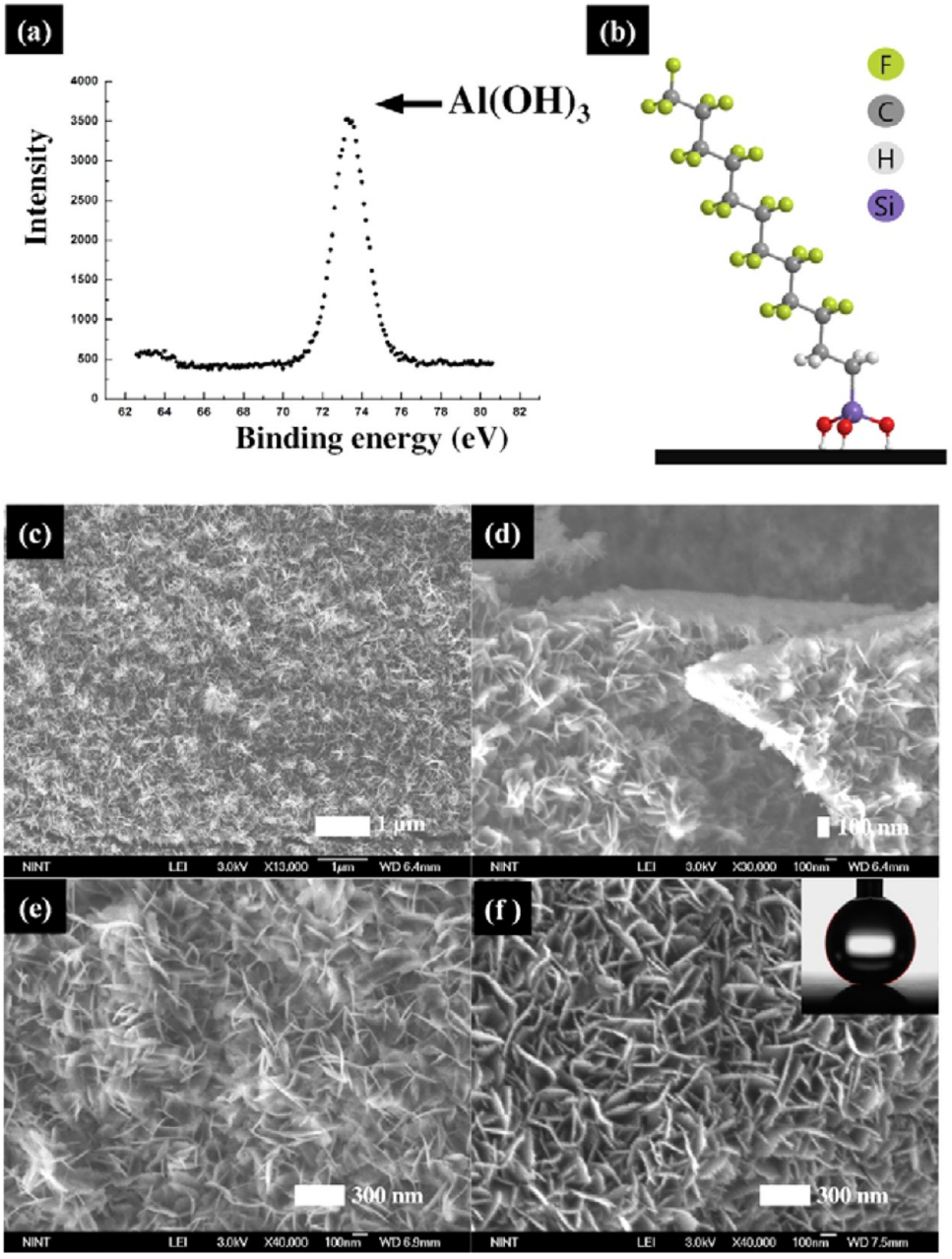

Figure 1. Chemical and geometrical characteristics of superhydrophobic Al surface after alkali treatment, boiling, and SAM coating. (a) XPS analysis for chemical characteristics after alkali treatment and boiling treatment and (b) remaining chemical groups on the surface after SAM coating, to which they impart hydrophobicity. SEM images of (c) top view, (d) tilted view for height of flakes, (e) magnified top view of (c), and (f) top view after SAM coating. After SAM coating, flakelike nanostructures remained covering the surface, and large numbers of sub-nanoscale flakes trap a large amount of air and lead to high static contact angle.

characteristics requires development of a superhydrophobic surface on which SPJ is better than on existing micro- or nanostructured surfaces.

To expand the advantages of a superhydrophobic surface for anti-icing applications, it should be achieved on a material like aluminum (Al) that has many industrial uses. Most previous research into self-propelled jumping and anti-icing surface has focused on gaining scientific understanding of SPJ. Some research obtained self-propelled jumping motion at relatively high S, but superhydrophobic surfaces that were fabricated were not suitable for industrial application because they require relatively expensive and time-consuming fabrication processes and are not applicable to real devices.[23,24] Herein, we introduce a very effective superhydrophobic Al surface for anti-icing applications. The prepared surface induces SPJ of condensate droplets at high S (S = 3.41, 6.39), and therefore is effective to delay or suppress frost formation.

2. EXPERIMENTAL SECTION

2.1. Fabrication of Superhydrophobic Aluminum Surface. Generally, superhydrophobicity is achieved chemically to prepare a surface with low surface energy and geometrically to produce a surface that has microstructures and/or nanostructures.[25,26] Al is smooth and intrinsically hydrophilic, so it must be modified both chemically and geometrically. Recently, some groups[27,28] introduced a simple

DOI: 10.1021/acsami.5b00292
ACS Appl. Mater. Interfaces 2015, 7, 7206−7213

Table 1. Mean ± Range Limits of Static, Advancing, and Receding Contact Angles on Untreated or Treated Al Surfaces According to Its Fabrication Conditions

specimen	NaOH time (min)	boiling time (min)	SAM coating	contact angle (deg) static	contact angle (deg) advancing	contact angle (deg) receding
bare	0	0	no	96.9 ± 0.3	105.0 ± 0.4	51.7 ± 6.5
hydrophilic	5	0	no	<10	11.5 ± 2.3	<5
hydrophobic	5	0	yes	138	154.3 ± 2.3	111.4 ± 4.3
superhydrophobic 1	5	5	yes	166 ± 5.7	168.7 ± 2.8	162.7 ± 1.3
superhydrophobic 2	5	30	yes	170.8 ± 1.6	178.8 ± 0.0	169.7 ± 1.0
superhydrophobic 3	5	60	yes	170.3 ± 2.0	178.5 ± 0.4	167.0 ± 1.6

method to fabricate an aluminum hydroxide layer by alkali treatment or nanostructures by boiling in water. On the basis of their method, we effectively achieved nanostructured superhydrophobic Al. The process to fabricate a superhydrophobic nanostructured surface consists of three steps: (1) alkali treatment to induce formation of an aluminum hydroxide ($Al(OH)_3$) layer, (2) boiling to induce formation of nanostructures, and (3) applying a self-assembled monolayer (SAM) coating with low surface energy.

Industrial-grade aluminum sheets (99.5%, 30 mm × 20 mm × 1 mm) were used in all experiments. The $Al(OH)_3$ layer was formed by dipping specimens in a 0.05 M NaOH solution at 80 °C for 5 min. The specimens were then immersed in boiling deionized water for 30 min; this process formed nanostructures on the surface. The specimens had a nanostructured $Al(OH)_3$ layer and was superhydrophilic. To render it superhydrophobic, a coating with low surface energy was applied by immersing it for 3 h in an *n*-hexane-based solution that contained 0.1% heptadecafluoro-1,1,2,2-tetrahydrodecyl-trichlorosilane (HDFS, Gelest), and then cleaning the surface using *n*-hexane and an HFE-7100-engineered solvent (3M).[25] As a result, a nanostructured superhydrophobic Al surface (NanoAl) was achieved.

The "Smooth" hydrophobic Al surface (SmooAl) was fabricated by alkali treatment and SAM coating. It was used as a standard for comparison for anti-icing characteristics; this is a typical smooth hydrophobic surface prepared by chemical modification for low surface energy.

2.2. Condensation and Icing Experiments. The specimens were mounted on a Peltier-based cooling system and cooled to −1 or −9 °C. The temperature reached the final temperature in less than 45 s. The experiments were conducted (1) at ambient temperature T of 25.5 ± 0.5 °C and relative humidity RH = 62 ± 2% (S = 3.41), or (2) at T = 23.3 ± 0.2 °C and RH = 70.5 ± 1.5% (S = 6.39). Al squares (20 mm × 20 mm) were placed vertically on a cooling stage. Water condensation and frosting were recorded at 200× magnification through a microscope (field of view 2 mm × 1.5 mm); movies were recorded at 30 fps.

The video recorded the middle of the specimen. Condensation characteristics including size of droplets and the number of droplets are manually investigated using ImageJ software. Frosting characteristics measuring speed of frost propagation is also measured using ImageJ. The propagation speed of frost propagation can be roughly quantified by dividing the proportion of the area covered by frozen droplets by freezing duration; frozen condensate droplets are confirmed by their opacity. The presented speeds are the averages obtained from propagation speeds in two time intervals. Each experiment was repeated several times.

3. RESULTS AND DISCUSSION

3.1. Chemical and Geometrical Characteristics of Superhydrophobic Al. Superhydrophobicity was obtained (Figure 1). The $Al(OH)_3$ layer was formed by alkali treatment and dipping in boiling water. In alkali treatment using NaOH solution, Al and its naturally oxidized surface Al_2O_3 react with NaOH solution as[29]

$$Al_2O_3 + 2NaOH + 3H_2O \rightarrow 2Al(OH)_4^- + 2NA^+ \quad (1)$$

$$2Al + 2NaOH + 6H_2O \rightarrow 2Al(OH)_4^- + 2Na^+ + 3H_2 \quad (2)$$

NaOH solution leads to significant supersaturation and rapid precipitation of $Al(OH)_3$ at an extreme pH level.[27] Because of the hydrophilic nature of aluminum, the $Al(OH)_3$ precipitates, attract water molecules, and form a gel. In the subsequent process of dipping in boiling water, the aluminate ions in the gelatinous layer are crystallized to $Al(OH)_3$.[27] The result can be expressed as[30]

$$Al(OH)_4 \rightarrow Al(OH)_3 + OH^- \quad (3)$$

The elemental composition of the modified Al surface (Figure 1a) was measured using X-ray photoelectron spectroscopy (XPS) analysis after alkali treatment and dipping in boiling water. The analysis detected a binding energy peak at 73.6 eV, which corresponds to $Al(OH)_3$. HDFS has chlorine as head groups and fluorine as tail groups; the head part of HDFS react with OH on the surface to form the SAM (Figure 1b). The fluorine tail groups cause hydrophobicity, so they impart low surface energy to the Al surface.

The surface morphologies (Figure 1c–f) of the modified Al surface were investigated using scanning electron microscopy (SEM). The top, tilted, and magnified-top view images (parts c, d, and e, respectively, of Figure 1) show specimens without SAM coating. Flakelike nanostructures cover the surface, and large numbers of subnanoscale flakes formed pores with sizes ~100 nm, which trap a large amount of air (Figure 1c–f, Figures S1 and S2 in the Supporting Information). These flakes were ~100 nm high (Figure 1d). Even after SAM coating, the scale of structures did not change, so the surface maintained its large number of 100 nm pores and sub-nanometer flakes (Figure 1e,f). These subnanoscale flakes enable water to barely touch the surface. As a result, flakelike nanostructures and fluorine covering the surface induced superhydrophobicity (Table 1; inset of Figure 1f).

The fabrication process for superhydrophobic Al is simple but effective, and has four advantages from the industrial perspective: (1) it can be used on arbitrarily shaped surfaces; (2) it can be realized over large areas; (3) it does not require additional high-temperature annealing or drying; (4) the growth mechanism of the nanostructure layer is self-limiting.

DOI: 10.1021/acsami.5b00292
ACS Appl. Mater. Interfaces 2015, 7, 7206–7213

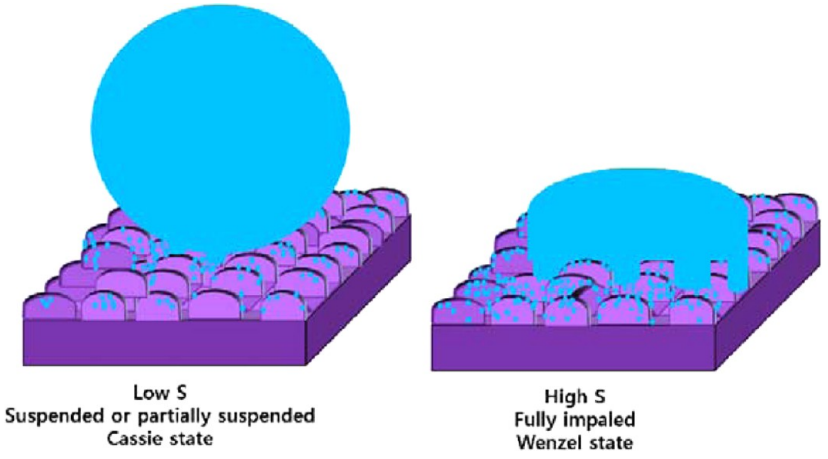

Figure 2. Schematic drawing of wetting mode according to degree of supersaturation (S).

This self-limiting growth mechanism forms a uniform nanostructure layer independent of boiling time, as demonstrated by SEM images and contact angle (CA) information obtained using a commercial CA measurement system (SmartDrop Lab, FEMTOFAB) (Figure S1 in the Supporting Information, Table 1).

3.2. Condensation Characteristics. When condensate droplets coalesce on a superhydrophobic surface that has extremely low adhesion, they present SPJ independent of gravity.[20,31] This phenomenon results from kinetic energy converted by excess of surface energy during the coalescence. The SPJ further enhances condensation heat transfer over conventional dropwise condensation and delays frost formation, so many researchers have attempted to fabricate superhydrophobic surfaces to sustain SPJ.[32] However, SPJ does not always happen on all of the superhydrophobic surface and is not always maintained. For example, dropwise condensation without SPJ is observed on diverse superhydrophobic surfaces[32−34] or SPJ does not occur if the humidity increases or the temperature of the substrate decreases even on the same superhydrophobic surface.[18,20] SPJ occurs on superhydrophobic surfaces that have extremely low adhesion, which is determined by the design of the surface and environmental conditions.

In this work, we used S to estimate the extent of condensation (i.e., nucleation density), which affects adhesion between condensate droplets and the surface. S can be controlled by changing the humidity or the temperature of the substrate. When S increases due to increase in humidity or decrease in temperature, condensate droplets are formed increasingly rigorously inside the structures of the superhydrophobic surface. As a result, the condensate droplets significantly alter the interfacial properties of the original superhydrophobic surface: it loses its low adhesion superhydrophobic properties.

For condensate droplets to show SPJ, released surface energy during coalescence is important, which is related to S. Zhao and co-workers[31] proposed a quantitative explanation of droplet jumping by understanding the relationship among participating energies. The approach is based on an equilibrium balance of surface energy, kinetic energy, and viscous dissipation energy. The released surface energy is converted to the kinetic energy of the merged droplet. From the mass balance among surface energy, kinetic energy, and viscous dissipation energy during coalescence of two condensate droplets, Zhao and co-workers acquired the kinetic energy resulting from a droplet coalescing on a superhydrophobic structured surface:

$$E_K = \gamma_{lv}\pi r^2\{(2 - 2^{2/3})(2 - 2\cos\theta) + [2^{2/3}(r_{fc}f_c\cos\theta_Y + f_c - 1) - 2(r_{fw}f_w\cos\theta_Y + f_w - 1)]\sin^2\theta\} - 64\pi\mu\sqrt{\frac{\gamma_{lv}r^3}{\rho}}$$

(γ, interfacial tension; l, liquid; s, solid; v, vapor; r, radius of condensate droplet; r_f, roughness ratio of the wet surface area; c, Cassie−Baxter; w, Wenzel; f, the fraction of the solid surface area wetted by the liquid; θ_Y, Young contact angle; μ, viscosity of the liquid; ρ, density).

To achieve SPJ, E_K must be greater than 0. Kinetic energy is released surface energy minus energy loss due to viscous dissipation, so for this system to achieve SPJ, the loss due to viscous dissipation must be reduced. This equation indicates that the kinetic energy required for SPJ is dependent on the size of the starting droplets and the wettability of the surface. The wettability of the surface is important for SPJ motion. SPJ cannot be realized when hydrophobicity is decreased. This decrease can occur as a result of environmental conditions: when the environmental conditions are appropriate to reach dew point, condensation occurs, in which condensate droplets fully or partially fill the air gaps among structures; this process increases the contact area and the adhesion force between condensate droplets and the surface.[35,36] When S is low, condensate droplets have relatively small contact and small adhesion (Figure 2). However, as S increases, condensate nucleation density is rigorously formed inside surface structure.[20] This process causes tiny condensate droplets to fill a greater proportion of the structures on the surface, thereby resulting in a pinned liquid film; that is, this process degrades hydrophobicity, increasing both the adhesion and the contact between surface and condensate droplets. Therefore, superhydrophobic surfaces do not present continuous SPJ after S increases beyond some limit.

Several studies have proved the importance of self-propelled jumping motion for anti-icing, antifogging, and enhanced heat-transfer applications.[17,37] But high-S environmental conditions, which can occur when humidity is high or temperature is low, hinder the ability of superhydrophobic surfaces to produce SPJ. However, on the prepared structured superhydrophobic aluminum surface, SPJ was observed at high S (S = 3.41 and 6.39) until the droplets froze (Figure 3). This indicates the prepared surface is effective for practical applications.

DOI: 10.1021/acsami.5b00292
ACS Appl. Mater. Interfaces 2015, 7, 7206−7213

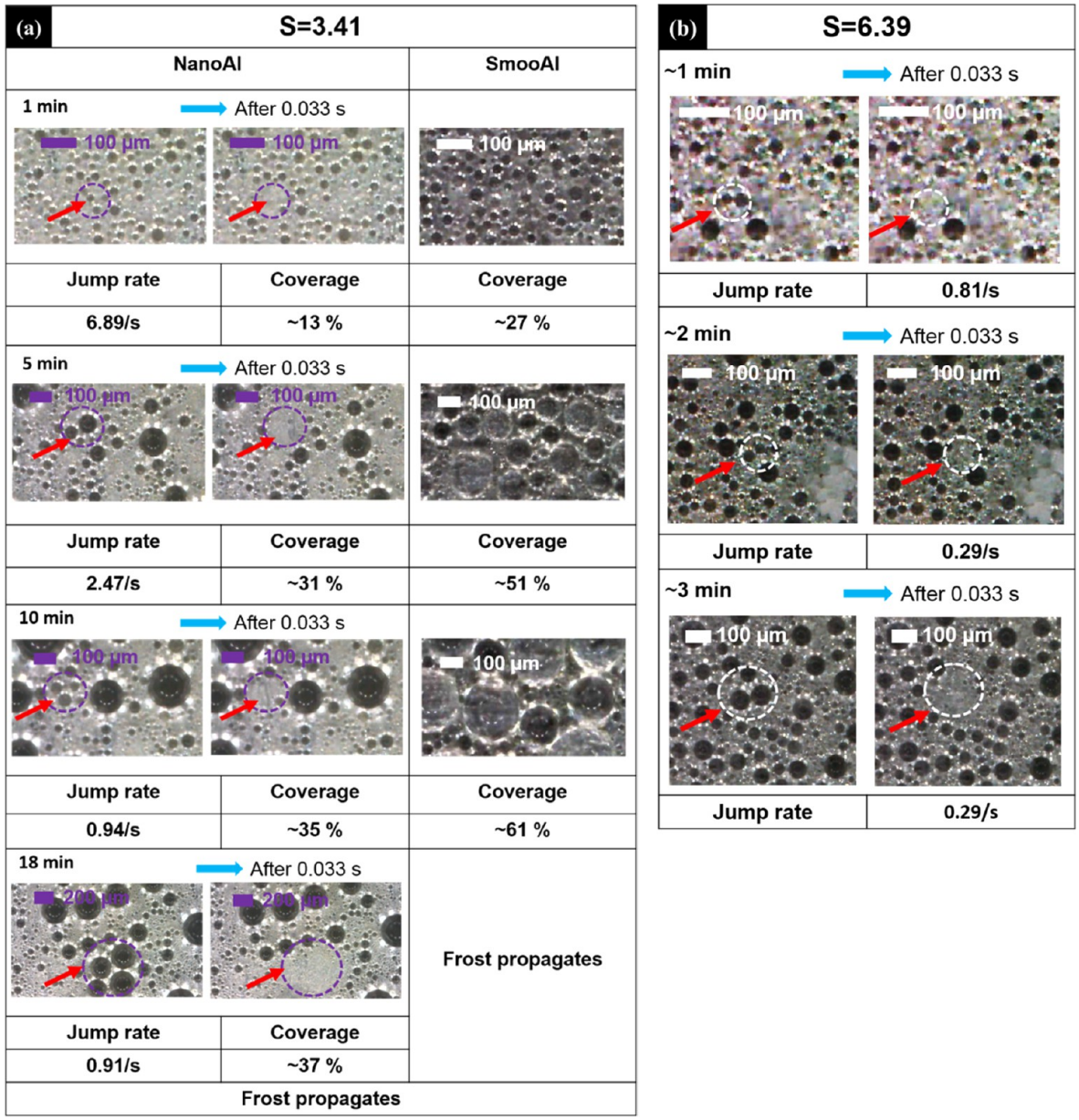

Figure 3. Self-propelled condensate jumping motion at (a) S = 3.41, (b) S = 6.39. Whether SPJ occurs or not and jump rate is dependent on S and surface wettability. NanoAl presents SPJ at high S; on SmooAl, no SPJ occurs. Low droplet growth rate and high jumping motion of low adhesive NanoAl enable low surface coverage of condensate droplets, resulting in retardation of frost formation.

To confirm the effect of anti-icing on nanostructured superhydrophobic Al surface, we compared the behavior of condensate droplets on NanoAl to those on SmooAl (Figure 3a). We also conducted condensation-based icing experiments with an Al surface which is geometrically intermediate between SmooAl and NanoAl (details in Supporting Information). Icing started after ~18 min on NanoAl and after 10 min SmooAl. SPJ was observed on NanoAl until icing began, but decreased over time. This decrease may occur because the increase in the adhesion of condensate droplets on the surface is much greater than the amount of jumping condensate water; consequently, the surface wetted gradually. Despite the reduced jump rate, it was continuous even in these high-S conditions because the surface did not undergo the transition from Cassie droplets to highly pinned Wenzel droplets, which completely wet the cavities of the structure.

A nanostructured superhydrophobic surface helps the growth of condensate droplets in a suspended Cassie state, in contrast to the Wenzel state on a microstructured superhydrophobic surface.[6,38−40] As S increases, the likelihood that the droplet will change from the Cassie state to the Wenzel state increases, as does the likelihood that the hydrophobicity will degenerate until SPJ is not possible. However, NanoAl allowed jumping motion at high S due to the small adhesion between the surface and the condensate droplets. NanoAl has nanostructures <100 nm in size (Figure 1); these extremely small nanostructures minimize the nucleation density of the condensate inside structures relative to the other micro- or nanostructured surface. The low nucleation density in the cavities of the structures enables most of the nucleating condensate droplets to grow over the structures in a suspended Cassie state; this process allows droplets on NanoAl to jump at high S.

DOI: 10.1021/acsami.5b00292
ACS Appl. Mater. Interfaces 2015, 7, 7206−7213

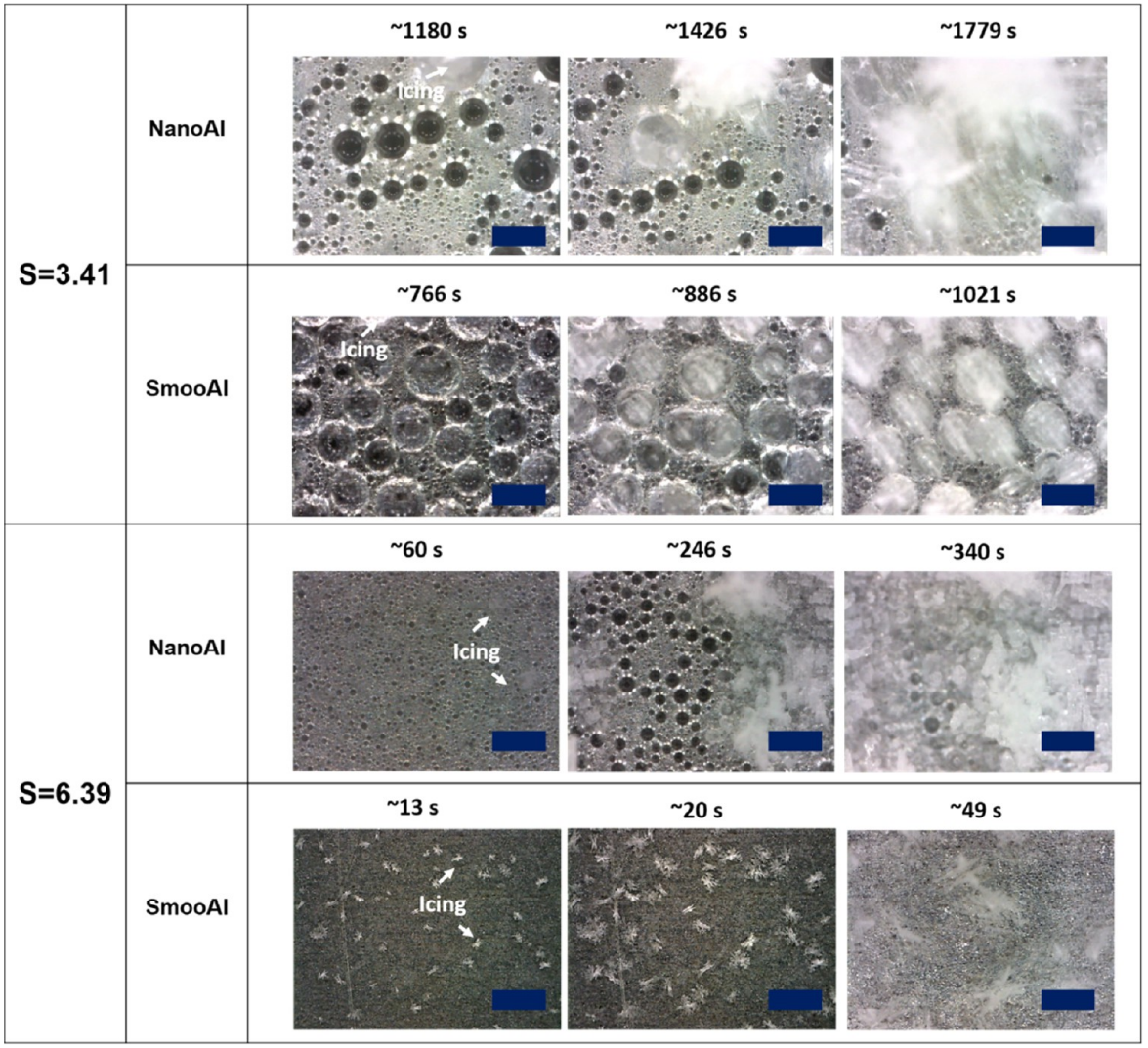

Figure 4. Time-lapse images of frost propagation after onset of freezing at S = 3.41 and S = 6.39. Frost propagates on SmooAl ~8.4 times and ~4.8 times faster than on NanoAl. Frost propagation is related to the distance among droplets. On the SmooAl surface having close distance among droplets, frost propagates faster than on NanoAl. Scale bar: 200 μm.

We observed jumping motion of droplets of sizes >100 μm. This observation of SPJ of such comparatively large droplets at high S reveals that the NanoAl surface has great potential for use in highly efficient removal of condensate droplets to reduce the cost of anti-icing treatments and to enhance heat transfer.

NanoAl and SmooAl differ in growth of condensate. The growth of condensate droplets follows a power law[41]

$$2r \sim t^{\alpha}$$

(r, radius of condensate droplets; t, time; α, growth law exponent dependent on the stage of condensation), where $\alpha \sim 0.56$ on NanoAl and $\alpha \sim 0.62$ SmooAl. The surface coverage (proportion of surface area covered by the droplets) of NanoAl and SmooAl reached ~37% and ~61%, respectively, before the onset of icing (S = 3.41). The SPJ event and slower growth rate in NanoAl attributed lower droplet coverage on NanoAl than on SmooAl at high S. This difference of coverage and droplet size has a great effect on frost propagation.

3.3. Anti-icing Characteristics. When water droplets accumulate by rapid condensation on a chilled surface, they stay and eventually freeze because they cannot roll off due to their size being less than capillary length.[3] Recently, a new approach to remove the condensed droplets and eventually prevent frost formation was proposed; this approach uses a suitably designed superhydrophobic surface on which condensate droplets spontaneously jump when they merge together, and on which dropwise condensation occurs as on a traditional hydrophobic surface.[17,37]

Frost is initiated at surface defects or at the outer edge corner of the substrate due to its geometrical singularity and low free energy barrier for heterogeneous nucleation.[37] As soon as frost starts to form, it propagates by formation of interbridges among neighboring droplets, which eventually cover the whole surface. Frost propagation can be delayed due to SPJ of condensate droplets, by which they limit interbridge formation.[17,37] Once nucleation of ice begins, ice growth is promoted by the Wegener-Bergeron-Findeisen process of desublimation in which the ice grows by feeding on the water vapor released by evaporation from neighboring droplets.[42] This process is attributed to the difference in saturated vapor pressure between ice and neighboring supercooled condensate droplet, which arises from the difference of bonding strengths of molecules between them. Air is near saturation for a water droplet, but is at supersaturation for ice. The driving force of the transport for

DOI: 10.1021/acsami.5b00292
ACS Appl. Mater. Interfaces 2015, 7, 7206−7213

ice growth is the gradient in supersaturation pressure and consequent movement of vapor by diffusion.[42] The frozen water grows to be ice dendrites; once one forms, its tip approaches neighboring condensate droplets, so it attracts additional vapor and grows further. As soon as it contacts the neighboring condensate droplets, it freezes almost immediately.[42] These processes at S = 3.41, 6.39 were monitored on the prepared NanoAl and SmooAl surfaces (Figure 4). The effect of self-propelled jumping on anti-icing was confirmed by comparing the speed of frost propagation on them. The first frozen droplet within the field of view at S = 3.41 was observed at 766 s on NanoAl, and at 11 801 s on SmooAl. The frozen droplets grew to become ice dendrites, and grown ice dendrites affected neighboring condensate droplets, thereby causing the frost to spread. The propagation speed of frost propagation can be roughly estimated by dividing the proportion of the area covered by frozen droplets by freezing duration. The frost propagated on the NanoAl surface at ∼2829.3 $\mu m^2/s$ and on the SmooAl at ∼24479.5 $\mu m^2/s$, i.e., was ∼8.6 times faster than on NanoAl. Likewise, the icing process was also investigated at S = 6.39. The speeds of frost propagation were 12253.3 $\mu m^2/s$ on the NanoAl and 61224.49 $\mu m^2/s$ on the SmooAl, which means that frost propagated on SmooAl ∼4.8 times faster than on NanoAl. This observation indicates the NanoAl surface effectively suppresses frost propagation by formation of interbridges. The difference in speed is attributed to the distance of interdroplets. To delay the frost propagation, neighboring droplets should be far apart. The distance between droplets can be described by droplet radius and surface coverage.[43]

$$\varepsilon^2 = \left(\frac{2R}{A}\right)^2$$

(ε, surface coverage; R, radius of droplet; A, mean distance between droplets). Although distances could not be calculated at S = 6.39 due to experimental limitations, the distances between condensate droplets at S = 3.41 was calculated using this equation; they were 42.2 μm on NanoAl and 30.7 μm on SmooAl. The lower droplet growth rate and SPJ on NanoAl compared to that on SmooAl reduces the coverage and droplet radius, and thereby successfully suppresses frost propagation by formation of interbridges among condensate droplets.

4. CONCLUSIONS

This work demonstrates superhydrophobic Al that can be used for antifrosting applications. The superhydrophobic Al is fabricated by very simple steps: alkali treatment, dipping in boiling water, and SAM coating. These processes yield conformal flakelike nanostructures with low surface energy; as a result, superhydrophobic Al is fabricated. This fabrication process can be applicable to arbitrarily shaped Al.

The superhydrophobic Al surface induces self-propelled jumping motion of condensate water droplets at high saturation S = 3.41 and 6.39. The self-propelled jumping and slow growth rate of frost nuclei on the surface successfully suppressed frost propagation. On the nanostructured Al surface, frost formation was delayed more than 4 times at S = 3.41 and S = 6.39 compared to the smooth Al surface. Therefore, superhydrophobic Al has many industrial applications including outdoor heat exchangers, which suffer from frosting problems in cold winters.

■ ASSOCIATED CONTENT

Supporting Information

SEM images of nanostructured aluminum surface corresponding to the kinds of surfaces in Table 1 are included to support the hypothesized self-limiting mechanism (Figure S1). To guide the preparation of an effective antifrosting surface, Supporting Information has images of morphology change according to boiling time and experimental results obtained by the surface under the middle stage of nanostructures (Figure S2). The antifrosting characteristics based on condensation were conducted with the surface selected due to its intermediate morphology (Figures S2 and S3). This material is available free of charge via the Internet at http://pubs.acs.org.

■ AUTHOR INFORMATION

Corresponding Author

*E-mail: joonwon@postech.ac.kr.

Notes

The authors declare no competing financial interest.

■ ACKNOWLEDGMENTS

In performing our paper, we received help from some respected persons and university that deserve our greatest gratitude. The completion of this paper gives us much pleasure. We show our gratitude to POSTECH, NINT, MNT, family, and God for giving us a good guideline and supports. Above all, we are very happy that we have grown intellectually while studying this topic. This work was partially supported by the National Research Foundation of Korea (NRF) grant funded by the Korea government (MSIP) (No. 2011-0030075). This work was partially supported by BioNano Health-Guard Research Center funded by the Ministry of Science, ICT & Future Planning (MSIP) of Korea as Global Frontier Project (Grant Number H-GUARD 2014M3A6B2060526).

■ REFERENCES

(1) Yao, Y.; Jiang, Y.; Deng, S.; Ma, Z. A Study on the Performance of the Airside Heat Exchanger under Frosting in an Air Source Heat Pump Water Heater/Chiller Unit. *Int. J. Heat Mass Transfer* **2004**, *47*, 3745−3756.

(2) Li, K.; Xu, S.; Shi, W.; He, M.; Li, H.; Li, S.; Zhou, X.; Wang, J.; Song, Y. Investigating the Effects of Solid Surfaces on Ice Nucleation. *Langmuir* **2012**, *28*, 10749−10754.

(3) Lv, J.; Song, Y.; Jiang, L.; Wang, J. Bio-Inspired Strategies for Anti-Icing. *ACS Nano* **2014**, *8*, 3152−3169.

(4) Boinovich, L. B.; Emelyanenko, A. M.; Ivanov, V. K.; Pashinin, A. S. Durable Icephobic Coating for Stainless Steel. *ACS Appl. Mater. Interfaces* **2013**, *5*, 2549−2554.

(5) Hewitt, N.; Huang, M. J. Defrost Cycle Performance for a Circular Shape Evaporator Air Source Heat Pump. *Int. J. Refrig.* **2008**, *31*, 444−452.

(6) Boreyko, J. B.; Srijanto, B. R.; Nguyen, T. D.; Vega, C.; Fuentes-Cabrera, M.; Collier, C. P. Dynamic Defrosting on Nanostructured Superhydrophobic Surfaces. *Langmuir* **2013**, *29*, 9516−9524.

(7) Lee, H.; Shin, J.; Ha, S.; Choi, B.; Lee, J. Frost Formation on a Plate with Different Surface Hydrophilicity. *Int. J. Heat Mass Transfer* **2004**, *47*, 4881−4893.

(8) Charpentier, T. V. J.; Neville, A.; Millner, P.; Hewson, R. W.; Morina, A. Development of Anti-Icing Materials by Chemical Tailoring of Hydrophobic Textured Metallic Surfaces. *J. Colloid Interface Sci.* **2013**, *394*, 539−544.

(9) Rykaczewski, K.; Anand, S.; Subramanyam, S. B.; Varanasi, K. K. Mechanism of Frost Formation on Lubricant-Impregnated Surfaces. *Langmuir* **2013**, *29*, 5230−5238.

DOI: 10.1021/acsami.5b00292
ACS Appl. Mater. Interfaces 2015, 7, 7206−7213

(10) Chen, J.; Liu, J.; He, M.; Li, K.; Cui, D.; Zhang, Q.; Zeng, X.; Zhang, Y.; Wang, J.; Song, Y. Superhydrophobic Surfaces Cannot Reduce Ice Adhesion. *Appl. Phys. Lett.* **2012**, *101*, 111603−111603-3.
(11) Kim, P.; Wong, T.-S.; Alvarenga, J.; Kreder, M. J.; Adorno-Martinez, W. E.; Aizenberg, J. Liquid-Infused Nanostructured Surfaces with Extreme Anti-Ice and Anti-Frost Performance. *ACS Nano* **2012**, *6*, 6569−6577.
(12) Sahoo, B. N.; Kandasubramanian, B. Recent Progress in Fabrication and Characterisation of Hierarchical Biomimetic Superhydrophobic Structures. *RSC Adv.* **2014**, *4*, 22053−22093.
(13) Mishchenko, L.; Hatton, B.; Bahadur, V.; Taylor, J. A.; Krupenkin, T.; Aizenberg, J. Design of Ice-Free Nanostructured Surfaces based on Repulsion of Impacting Water Droplets. *ACS Nano* **2010**, *4*, 7699−7707.
(14) Maitra, T.; Tiwari, M. K.; Antonini, C.; Schoch, P.; Jung, S.; Eberle, P.; Poulikakos, D. On the Nanoengineering of Superhydrophobic and Impalement Resistant Surface Textures below the Freezing Temperature. *Nano Lett.* **2014**, *14*, 172−182.
(15) Guo, P.; Zheng, Y.; Wen, M.; Song, C.; Lin, Y.; Jiang, L. Icephobic/Anti-Icing Properties of Micro/Nanostructured Surfaces. *Adv. Mater.* **2012**, *24*, 2642−2648.
(16) He, M.; Wang, J.; Li, H.; Jin, X.; Wang, J.; Liu, B.; Song, Y. Super-Hydrophobic Film Retards Frost Formation. *Soft Matter* **2010**, *6*, 2396−2399.
(17) Boreyko, J. B.; Collier, C. P. Delayed Frost Growth on Jumping-Drop Superhydrophobic Surfaces. *ACS Nano* **2013**, *7*, 1618−1627.
(18) Zhang, Q.; He, M.; Chen, J.; Wang, J.; Song, Y.; Jiang, L. Anti-Icing Surfaces based on Enhanced Self-Propelled Jumping of Condensed Water Microdroplets. *Chem. Commun.* **2013**, *49*, 4516−4518.
(19) Xu, Q.; Li, J.; Tian, J.; Zhu, J.; Gao, X. Energy-Effective Frost-Free Coatings Based on Superhydrophobic Aligned Nanocones. *ACS Appl. Mater. Interfaces* **2014**, *6*, 8976−8980.
(20) Miljkovic, N.; Enright, R.; Nam, Y.; Lopez, K.; Dou, N.; Sack, J.; Wang, E. N. Jumping-Droplet-Enhanced Condensation on Scalable Superhydrophobic Nanostructured Surfaces. *Nano Lett.* **2013**, *13*, 179−187.
(21) He, M.; Zhou, X.; Zeng, X.; Cui, D.; Zhang, Q.; Chen, J.; Li, H.; Wang, J.; Cao, Z.; Song, Y.; Jiang, L. Hierarchically Structured Porous Aluminum Surfaces for High-Efficient Removal of Condensed Water. *Soft Matter* **2012**, *8*, 6680−6683.
(22) Boreyko, J.; Chen, C.-H. Self-Propelled Dropwise Condensate on Superhydrophobic Surfaces. *Phys. Rev. Lett.* **2009**, *103*, 184501.
(23) Alizadeh, A.; Yamada, M.; Li, R.; Shang, W.; Otta, S.; Zhong, S.; Ge, L.; Dhinojwala, A.; Conway, K. R.; Bahadur, V.; Vinciquerra, A. J.; Stephens, B.; Blohm, M. L. Dynamics of Ice Nucleation on Water Repellent Surfaces. *Langmuir* **2012**, *28*, 3180−3186.
(24) Stone, H. A. Ice-Phobic Surfaces That Are Wet. *ACS Nano* **2012**, *6*, 6536−6540.
(25) Kim, A.; Kim, H.; Lee, C.; Kim, J. Effective Three-Dimensional Superhydrophobic Aerogel-Coated Channel for High Efficiency Water-Droplet Transport. *Appl. Phys. Lett.* **2014**, *104*, 081601−081604.
(26) Bhushan, B.; Chae Jung, Y. Wetting Study of Patterned Surfaces for Superhydrophobicity. *Ultramicroscopy* **2007**, *107*, 1033−1041.
(27) Seo, Y. I.; Lee, Y. J.; Kim, D.-G.; Lee, K. H.; Kim, Y. D. Mechanism of Aluminum Hydroxide Layer Formation by Surface Modification of Aluminum. *Appl. Surf. Sci.* **2010**, *256*, 4434−4437.
(28) He, M.; Zhang, Q.; Zeng, X.; Cui, D.; Chen, J.; Li, H.; Wang, J.; Song, Y. Hierarchical Porous Surface for Efficiently Controlling Microdroplets' Self-Removal. *Adv. Mater.* **2013**, *25*, 2291−2295.
(29) Seo, Y. I.; Lee, Y. J.; Hong, K. H.; Chang, D.; Kim, D.-G.; Lee, K. H.; Kim, Y. D. Phosphate Filtering Characteristics of a Hybridized Porous Al Alloy Prepared by Surface Modification. *J. Hazard. Mater.* **2010**, *173*, 789−793.
(30) Loh, J. S. C.; Fogg, A. M.; Watling, H. R.; Parkinson, G. M.; O'Hare, D. A Kinetic Investigation of Gibbsite Precipitation using in situ Time Resolved Energy Dispersive X-ray Diffraction. *Phys. Chem. Chem. Phys.* **2000**, *2*, 3597−3604.
(31) Wang, F.-C.; Yang, F.; Zhao, Y.-P. Size Effect on the Coalescence-Induced Self-Propelled Droplet. *Appl. Phys. Lett.* **2011**, *98*, 053112.
(32) Miljkovic, N.; Enright, R.; Wang, E. N. Effect of Droplet Morphology on Growth Dynamics and Heat Transfer during Condensation on Superhydrophobic Nanostructured Surfaces. *ACS Nano* **2012**, *6*, 1776−1785.
(33) Chen, C.-H.; Cai, Q.; Tsai, C.; Chen, C.-L.; Xiong, G.; Yu, Y.; Ren, Z. Dropwise Condensation on Superhydrophobic Surfaces with Two-Tier Roughness. *Appl. Phys. Lett.* **2007**, *90*, 173108.
(34) Zhang, Q.; He, M.; Xeng, X.; Li, K.; Cui, D.; Chen, J.; Wang, J.; Song, Y.; Jiang, L. Condensation Mode Determines the Freezing of Condensed Water on Solid Surfaces. *Soft Matter* **2012**, *8*, 8285−8288.
(35) Park, K.-M.; Lee, B.-S.; Youk, J. H.; Lee, J.; Yu, W.-R. Moisture Condensation Behavior of Hierarchically Carbon Nanotube-Grafted Carbon Nanofibers. *ACS Appl. Mater. Interfaces* **2013**, *5*, 11115−11122.
(36) Han Yeong, Y.; Steele, A.; Loth, E.; Bayer, I.; De Combarieu, G.; Lakeman, C. Temperature and Humidity Effects on Superhydrophobicity of Nanocomposite Coatings. *Appl. Phys. Lett.* **2012**, *100*, 053112.
(37) Chen, X.; Ma, R.; Zhou, H.; Zhou, X.; Che, L.; Yao, S.; Wang, Z. Activating the Microscale Edge Effect in a Hierarchical Surface for Frosting Suppression and Defrosting Promotion. *Sci. Rep.* **2013**, *3*, 2515.
(38) Rykaczewski, K. Microdroplet Growth Mechanism during Water Condensation on Superhydrophobic Surfaces. *Langmuir* **2012**, *28*, 7720−7729.
(39) Rykaczewski, K.; Osborn, W. A.; Chinn, J.; Walker, M. L.; Scott, J. H. J.; Jones, W.; Hao, C.; Yao, S.; Wang, Z. How Nanorough is Rough enough to Make a Surface Superhydrophobic during Water Condensation? *Soft Matter* **2012**, *8*, 8786.
(40) Lo, C.-W.; Wang, C.-C.; Lu, M.-C. Scale Effect on Dropwise Condensation on Superhydrophobic Surfaces. *ACS Appl. Mater. Interfaces* **2014**, *6*, 14353−14359.
(41) Beysens, D. The Formation of Dew. *Atmos. Res.* **1995**, *39*, 215−237.
(42) Guadarrama-Cetina, J.; Mongruel, A.; González-Viñas, W.; Beysens, D. Percolation-Induced Frost Formation. *Europhys. Lett.* **2013**, *101*, 16009.
(43) Beysens, D.; Knobler, C. Growth of Breath Figures. *Phys. Rev. Lett.* **1986**, *57*, 1433−1436.

DOI: 10.1021/acsami.5b00292
ACS Appl. Mater. Interfaces 2015, 7, 7206−7213